AIAA SciTech Forum
11–15 & 19–21 January 2021, VIRTUAL EVENT
AIAA Scitech 2021 Forum

10.2514/6.2021-0443

Hierarchical Nano- and Micro-engineered Interlaminar Reinforcement of Advanced Aerospace Grade Composites with Carbon Nanotube Arrays

Jeonyoon Lee* and Luiz H. Acauan†
Massachusetts Institute of Technology, Cambridge, MA, 02139, United States

Estelle Kalfon-Cohen‡ and Seth S. Kessler§
Metis Design Corporation, Boston, 02114, United States

Brian L. Wardle¶
Massachusetts Institute of Technology, Cambridge, MA, 02139, United States

Several novel next-generation composite architectures are demonstrated by introducing hierarchical architectures of vertically aligned carbon nanotube (VACNT) arrays. Here, we integrate buckling and patterning of VACNT arrays with advanced aerospace-grade carbon fiber polymer-matrix composites to introduce multi-level hierarchy into the interlaminar regions of composite laminates comprised of unidirectional IM7/8552 plies. The integration of buckled and patterned VACNTs shows ~7% increase in static interlaminar shear strength and ~224% increase in fatigue life across several load levels under short beam shear tests, when compared to the baseline unreinforced system. This hierarchical nano-engineered interlaminar reinforcement alters the damage modes, leading to a significant increase in structural strength over the conventional composites, beyond the unbuckled VACNT system. This work further demonstrates the ability to utilize structural instability of the nanoscale fibers at the microscale. In addition to the improvements in mechanical performance, the hierarchical composites with these micro-buckled nanoscale arrays are expected to be extended to multifunctional purposes beyond structural applications.

I. Nomenclature

CNT	=	carbon nanotube
SBS	=	short beam shear
UD	=	unidirectional
σ_{SBS}	=	short-beam strength
P_{f}	=	load at the failure observed during the short beam shear test
w_{SBS}	=	width of the short beam shear specimen
t_{SBS}	=	thickness of the short beam shear specimen

II. Introduction

Advanced composite materials comprised of laminated architectures have been widely used in many fields, especially in aerospace applications, due to their outstanding mechanical properties, which outperform the estimated properties from the rule of mixture of their constituents [1]. The evolution of laminated composite materials has opened new vistas in the development of aircraft in the industry, as these materials offer a weight reduction that can increase the

*Postdoctoral Associate, Department of Aeronautics and Astronautics.
†Research Scientist, Department of Aeronautics and Astronautics.
‡Director of Multifunctional Materials.
§President and Chief Executive Officer.
¶Professor, Department of Aeronautics and Astronautics and Mechanical Engineering, AIAA Associate Fellow.

payload. A unique feature of laminated composites is the layered architecture of stacked prepreg plies consolidated under high processing conditions, which yield high performance throughout the part. However, such advanced composite materials show relatively low through-thickness mechanical strength due to the resin-rich interfaces at the interlaminar regions, and therefore composite laminates are vulnerable to delamination failure modes [2]. To enhance the mechanical performance in through-thickness direction, several approaches have been introduced, including stitching, z-pinning, and 3D weaving [3–7]. However, these approaches use pins and stitches that are comparatively large to the composite microfibers; therefore, the unavoidable artifacts such as microfiber movement and damage, and in-plane microfiber volume loss are introduced as damage precursors, as such the pins and stitches physically penetrate the composite laminates. Consequently, in-plane properties of laminates are often significantly reduced. In recent decades, nanomaterials have been of interest as enhancing fillers for improving the interlaminar mechanical properties of laminates [8, 9]. Nanoscale reinforcements, such as carbon nanotubes (CNTs) and graphene nanoplatelets, have exceptional mechanical properties better than microfibers, and their nanoscale dimension could reinforce the laminates without degrading the in-plane properties. Furthermore, positive scale effects in bridging toughening have been reported [10, 11].

Hierarchical design composites can further amplify the advantageous properties of composite materials [9]. The benefits of the structural hierarchy have been demonstrated in nature, especially in seashells. Seashells are comprised of two ingredients (i.e., aragonite and organic biopolymer), which are arranged hierarchically into multiscale architecture; thus, they exhibit several times increase in strength and thousandfold enhancement in toughness when compared to their components [12]. Inspired by this hierarchical multiscale architecture in nature, we introduce nano- and micro-engineered interlaminar reinforcement, which has a multi-level hierarchy, into the ply interfaces to improve further the mechanical properties of advanced aerospace-grade composites (i.e., HexPly IM7/8552). The multi-level hierarchy comprises two architectures: (1) buckling of VACNT arrays and (2) patterning of VACNT arrays. Researchers have found that aligned CNTs form a unique rippled folding shape under compression, while maintaining their alignment [13–15]. Besides, it has been demonstrated that a wavy fiber dissipates substantially more energy when being pulled out from a matrix compared to its straight counterpart, which directly translates to the significant fracture toughness of the composite materials [16, 17]. The patterning of VACNT is introduced to facilitate the possibility of the bridging effect of carbon microfibers in the interlaminar regions. The current work includes the study on the effects of buckling and patterning of VACNT (nanostitch 2.0), comparing to the VACNT without patterns (nanostitch 1.0).

III. Experimental

The synthesis and preparation of the several different kinds of nanostitch, fabrication of the nanostitch-integrated composite laminates, and mechanical testing methods for evaluation are described in this section.

A. Synthesis and Characterization of nanostitch 1.0 and 2.0

To synthesize VACNT arrays, a thermal catalytic chemical vapor deposition process was used with a quartz tube furnace of 44 mm inner diameter at atmospheric pressure, which is similar to a previously reported process. The catalyst is 1 nm Fe, supported on 10 nm Al_2O_3. Ethylene was used as the carbon source, and water of 600 ppm was added to the helium gas. In order to achieve nanostitch 2.0, the wafer was patterned with photoresist by standard lithography before catalyst deposition, and the catalyst is patterned by lift-off of the photoresist in acetone. The sizes of the pattern are 50 μm × 50 μm squares with a 2 μm gaps. As-grown CNT arrays having a height of 20 μm were used for nanostitch 1.0. Patterned as-grown CNT arrays having the height of 40 μm were used for nanostitch 2.0 so that the expected volume fraction of nanostitch 2.0 is twice of nanostitch 1.0. For both cases, the wafer size of 30 mm × 40 mm was utilized with a 2-inch diameter quartz boat. Figure 1 (a) and (b) show the top-down view of 20 μm-tall VACNT for nanostitch 1.0 and 40 μm-tall VACNT with 50 μm × 50 μm square-patterns for nanostitch 2.0. The as-grown CNT arrays consist of multiwalled CNTs with 3-7 walls with an average inner and outer diameter of ≈5.1 nm and ≈7.8 nm. The volume fraction of CNT arrays corresponded to ≈1.0% with an intrinsic CNT density of ≈1.6 g/cm^3 and an average inter-CNT spacing of ≈59 nm [18]. The 40 μm patterned VACNT arrays for nanostitch 2.0 were pre-buckled by a fixed force of 100 N with a bare silicon wafer before the transfer process on to the surface of prepreg such that the morphology of the patterned VACNT arrays can be uniform. Figure 1 (c-f) present the scanning electron microscopy (SEM) images of patterned VACNT arrays before and after the buckling process. The 40 μm VACNTs were found to be compressed to ~10 μm due to the pre-buckling process. As presented in Figure 1 (e) and (f), the VACNT arrays were buckled and formed the rippled folding shapes.

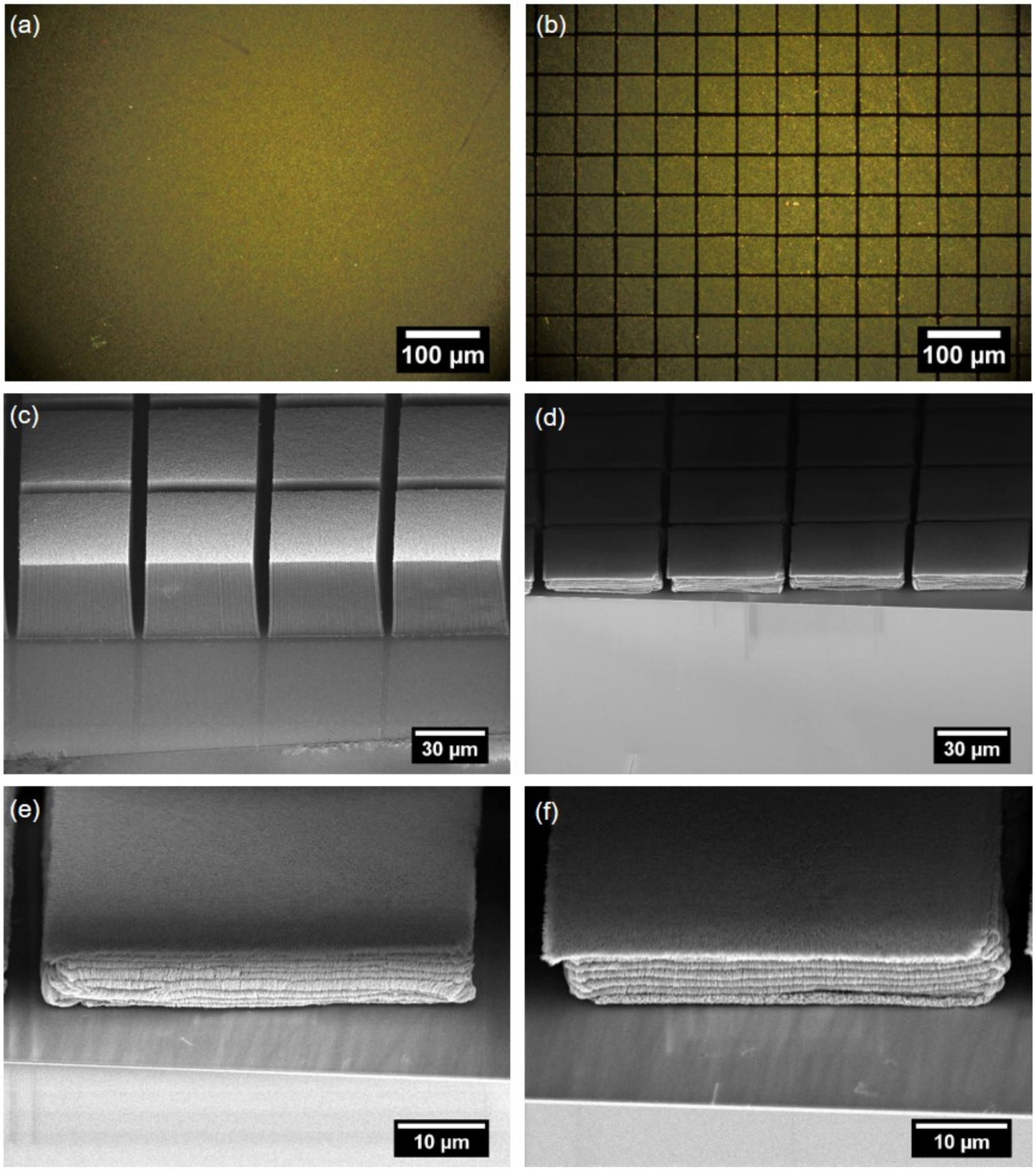

Fig. 1 Morphologies of nanostitch 1.0 and 2.0. Top-down optical micrographs of (a) 20 μm vertically aligned CNT for nanostitch 1.0 and (b) 40 μm vertically aligned CNT with 50 μm × 50 μm square-patterns and 2 μm gaps for nanostitch 2.0. SEM images of buckled and patterned arrays of VACNT arrays: (c) VACNTs before buckling showing aligned nanostructures, (d) VACNTs after buckling showing the rippled folding shapes, (e-f) magnified individual buckled VACNT arrays at different locations. The VACNTs were also effectively densified during the buckling process.

B. Composite Fabrication

In order to compare the effect of different types of interlaminar reinforcement, composite laminates with three different configurations were manufactured as follows: (1) baseline without any interlaminar reinforcement, (2) nanostitch 1.0 with 20 μm-tall VACNT, (3) nanostitch 2.0 with 40 μm-tall patterned VACNT having 50 μm × 50 μm squares with a 2 μm gap, respectively. The prepared nanostitches were integrated into the aerospace-grade laminated carbon fiber reinforced composites (i.e., unidirectional epoxy prepreg IM7/8552, Hexcel). The nanostitches were placed at all ply interfaces. The transfer of nanostitches was conducted by manually lightly compressing them to the surface of prepregs during the composite layup procedure, creating the nanostitch architecture in the interlaminar regions. The laminates were in a 16-ply quasi-isotropic layup ($[0/90/+45/-45]_{2S}$, and small angles (±2°) between the -45 plies at the middle of the laminates were introduced intentionally to avoid fiber nesting [19]. The laminates were cured in an autoclave at the Advanced Technology and Academic Center (ATAC) at the Great Bay Community College, following the manufacturer recommend cure cycle: 7 bar of total pressure at 3 °C/min to 110 °C, hold for 1 hour, ramp up again at 3 °C/min to 180 °C, hold for 2 hours, cool down at 5 °C/min to 60 °C and vent pressure, let cool down to room temperature. Once the laminates were cured, they have trimmed into 14.6 mm × 4.8 mm coupons for the short beam shear testing.

C. Static and Fatigue Short Beam Shear Test

The static short beam shear (SBS) test was conducted following the ASTM standard D2344 [20] to assess the interlaminar shear strength. The dimension of a specimen was nominally 14.4 mm × 4.8 mm × 2.4 mm (L × W × t), and these specimens were taken from the fabricated 6-inch × 6-inch quasi-isotropic laminates with and without interlaminar reinforcements. The specimens were cut with a diamond band saw, and the machined laminate edges were polished with 600, 800, 1200, and 2400 grit sandpapers to avoid rough or uneven surfaces. As prescribed in ASTM D2344, a three-point bend fixture with a 6 mm diameter loading nose, 3 mm diameter steel cylinder supports, and a span length of 8 mm was used. During the tests, the force applied to the specimen was monitored at a rate of crosshead movement of 1.0 mm/min applied by a Zwick/Roell Z010 mechanical testing machine. The short-beam strength (σ_{SBS}) was calculated using the equation:

$$\sigma_{\text{SBS}} = 0.75 \times \frac{P_{\text{f}}}{w_{\text{SBS}} \times t_{\text{SBS}}} \tag{1}$$

where P_{f}, w_{SBS}, and t_{SBS} are the load at the failure observed during the test, the width, and the thickness of the specimen, respectively. For the fatigue SBS testing, the static SBS test configuration was utilized, principally adopting the ASTM D2344 Standard. In other words, the test configuration for fatigue is the same as the static test, except the monotonic loading replaced with a cyclic sinusoidal stress-controlled loading. The fatigue testing was conducted using an Instron fatigue system (model 1332) with a Wyoming test fixture (WTF-SB made of 17-4PH steel) (see Figure 2 (a)). In order to remove possible crack initiators on the surfaces of specimens, the SBS specimens are further polished in the following order: 600, 800, 1200, 2400 grit sandpapers, and 1 µm alumina polishing suspension. Three cases (i.e., baseline, nanostitch 1.0, and nanostitch 2.0) were subjected to the fatigue SBS test. The specimens were loaded at maximum stresses that are 90%, 80%, 70%, and 60% of the static SBS strength of the baseline (~96.83 MPa), and the stress ratio (or R-ratio) of 0.1 was used in this study (see Figure 2 (b)). Three samples were tested for each stress level. The frequency of the applied stress was 10 Hz. The specimens are considered failed under two conditions: (1) when the specimen failed catastrophically, or (2) when the maximum displacement in a load cycle, as measured from the test machine crosshead, had changed by more than 20%, indicating a significant damage event. The failure cycle was

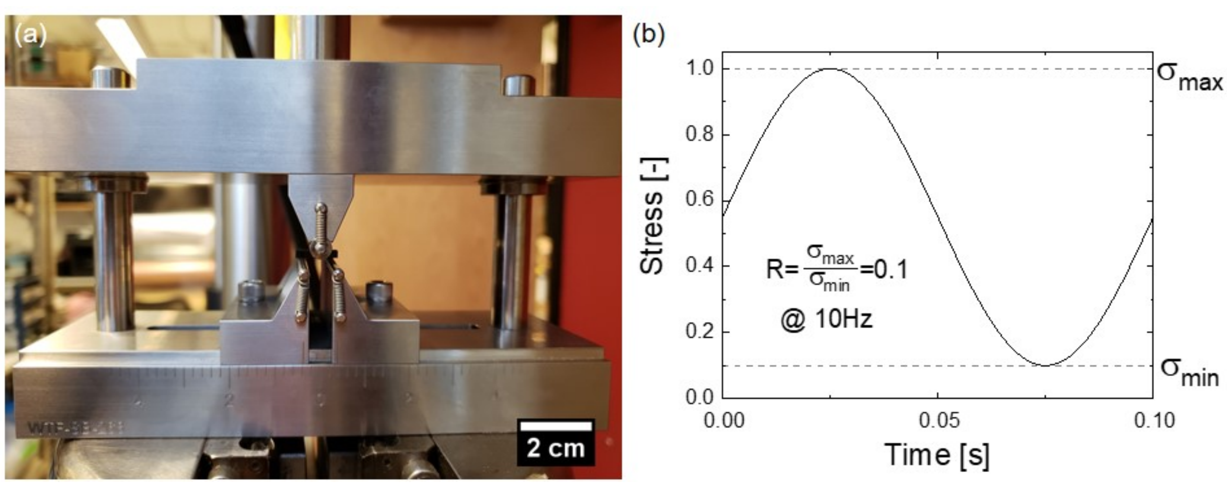

Fig. 2 Experimental setup for fatigue short beam shear test. (a) Instron fatigue system (model 1332) with a Wyoming test fixture (WTF-SB made of 17-4PH steel), and (b) applied stress during fatigue test (cyclic sinusoidal stress-controlled loading with R-ratio of 0.1 at 10 Hz)

recorded for each load level and used to calculate the classical stress vs. life cycles curve (S-N curve).

D. Micro-computed Tomography (μCT) on *Post Mortem* Specimens

From a structural mechanics point of view, it is important to examine the modes of failure in the tested composites to understand the effect of the interlaminar reinforcements. To compare the failure mode of the SBS specimens, μCT images of specimens were acquired by ZEISS Xradia 520 Versa 3D X-ray Microscopy. An isotropic voxel size of 8.5 μm was used to capture the cracks in a whole SBS specimen. For each scan, 3201 2D X-ray projections were taken with μCT parameters as follows: X-ray source energy of 80 kV and 7 W, exposure time of 1 second, and angular range of -180°to 180°. Additionally, a 150 μm silicon dioxide filter was used in all scans to mitigate the beam hardening effect. The 3D reconstructions were generated using the embedded ZEISS reconstruction software. Once 3D volumes were reconstructed, the volumes were processed with ImageJ to acquire 2D cross-sections. The cracks can be detected by applying a threshold filter on a histogram of the pixel intensity values via ImageJ. The intensity histogram exhibits a distinct bimodal distribution due to the cracks; the peak with a lower intensity corresponds to the cracks, while the peak with a higher intensity corresponds to the fiber and matrix.

IV. Results and Discussion

The interlaminar regions of the fabricated composite laminates are examined by scanning electron microscopy to evaluate if the buckled morphologies of VACNTs remain after the fabrication and if the characteristics of the interlaminar region change. The static and fatigue SBS test are presented here. To explore the origins of strength improvements by nanostitch, the *post mortem* SBS specimens were imaged via 3D micro-computed tomography using a lab-based 3D X-ray microscope.

A. Morphologies of the Interlaminar Region

SEM images of the composite laminates were taken to characterize the nanostitch-introduced interlaminar region. Figure 3 shows the comparison between the cross-sections of the baseline, nanostitch 1.0, and nanostitch 2.0 composites.

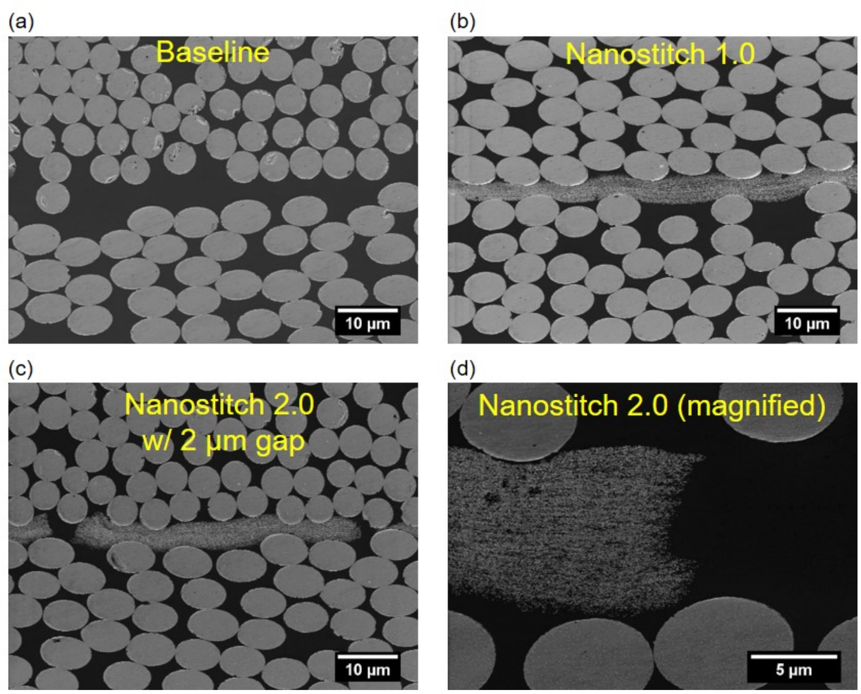

Fig. 3 Comparison of interlaminar regions. SEM image showing the interlaminar region of (a) baseline, (b) nanostitch 1.0, and (c) nanostitch 2.0. (d) Magnified image of nanostitch 2.0 showing that the rippled buckling and the alignment are maintained.

As presented in Figure 3 (a-c), there was no significant difference in the interlaminar regions among the three cases: the VACNT arrays used for nanostitch 1.0 and 2.0 were compressed down to ~5 μm by the applied pressure from the autoclave during the cure cycle, and therefore the interlaminar thickness remains the same despite the insertion of VACNT arrays. Given that the final thicknesses of the arrays of nanostitch 1.0 and nanostitch 2.0 are similar, the volume fraction of nanostitch 2.0 is twice higher than that of nanostitch 1.0. Of note, when VACNT arrays taller than 20 μm are used for nanostitch 1.0, an increase in the interlaminar thickness was reported [21], which may negatively alter the mechanical performance of a reinforced laminate due to the geometrical change. Therefore, this result supports that nanostitch 2.0 is the way to achieve interlaminar reinforcement in a higher volume fraction, which was not available in a single-level hierarchical structure (i.e., nanostitch 1.0). Besides, as shown in Figure 3 (d), the rippled folding shapes of the VACNTs were maintained even after they were introduced into the interlaminar region and underwent the curing process (7 bar of applied pressure at 180 °C).

B. Static and Fatigue Short Beam Shear Strength

The results of short beam shear (SBS) tests were evaluated to compare the mechanical properties of laminates cured under different reinforcing conditions. In the SBS test, five specimens were tested for each case. Figure 4 exhibits the short-beam strength of each reinforcement condition. In all cases, the interlaminar shear failure was observed among several failure modes described in the standard ASTM D2344. The baseline specimens presented the short-beam strength of 96.83 ± 1.35 MPa (Mean ± SE). Of note, it is previously reported that IM7/8552 laminates have short-beam shear strengths of ≈118 MPa and ≈93.5 MPa in unidirectional ($[0]_{32}$) and quasi-isotropic ($[0/90/\pm45/90/0/\pm45]_S$) layups, respectively [21]. The nanostitch 1.0 specimens showed a short-beam strength of 100.95 ± 1.39 MPa, which is ~4% increase over the baseline. In nanostitch 2.0, a short-beam strength of 104.02 ± 2.24 MPa was observed, a ~7% increase over the baseline. Considering the standard errors, nanostitch 1.0 and nanostitch 2.0 showed statically significant increases, compared to the baseline.

Figure 5 presents the number of cycles plotted against the maximum stress. In both cases (i.e., nanostitch 1.0 and nanostitch 2.0), statistically significant fatigue life enhancement was observed at 90%, 80%, and 60% load levels, compared to baseline. On average across the stress levels tested (90%, 80%, 70%, and 60% of SBS static strength), the nanostitch 1.0 and nanostitch 2.0 specimens exhibited extended fatigue life increased by 142% and 224%, respectively.

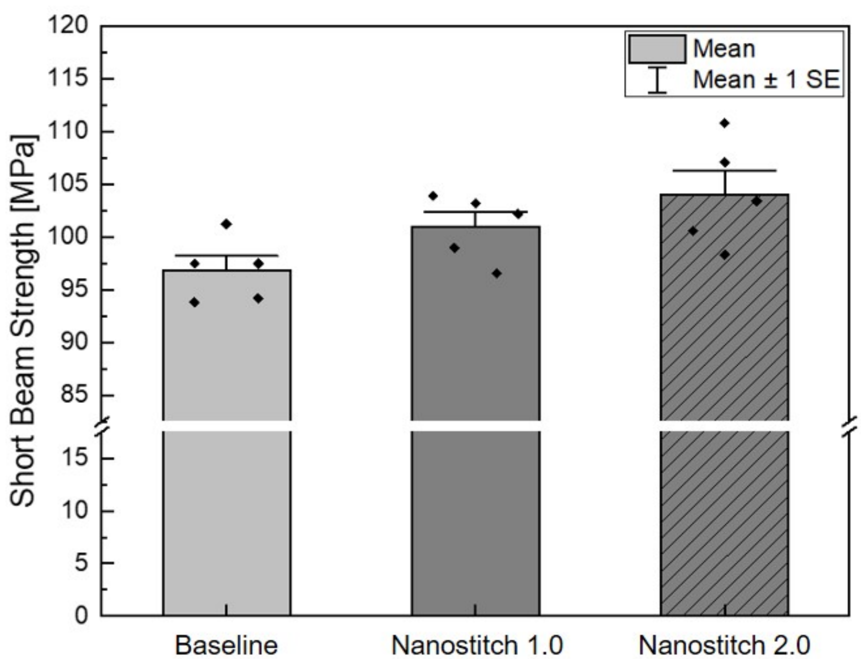

Fig. 4 Short-beam strength results for baseline, nanostitch 1.0 and nanostitch 2.0. The nanostitch 1.0 composites showed a ~4% increase over the baseline, and the nanostitch 2.0 composites showed a ~7% increase over the baseline. Both of them are statically significant.

Table 1 Short beam shear fatigue life of baseline, nanostitch 1.0, and nanostitch 2.0 under 60% to 90% of static strength, and fatigue life increase over baseline. * indicates statistically significant compared to baseline.

Stress Level	Fatigue Life Cycles (Mean±SE)			Fatigue Life Increase Over Baseline (%)	
	Baseline	Nanostitch 1.0	Nanostitch 2.0	Nanostitch 1.0	Nanostitch 2.0
90%	231 ± 73	663 ± 187	825 ± 148	187 *	257 *
80%	1365 ± 220	3724 ± 992	5420 ± 1218	173 *	297 *
70%	14342 ± 5615	23512 ± 11710	34036 ± 22656	64	137
60%	233423 ± 56493	568590 ± 232240	708255 ± 175074	144 *	203 *
Mean				142	224

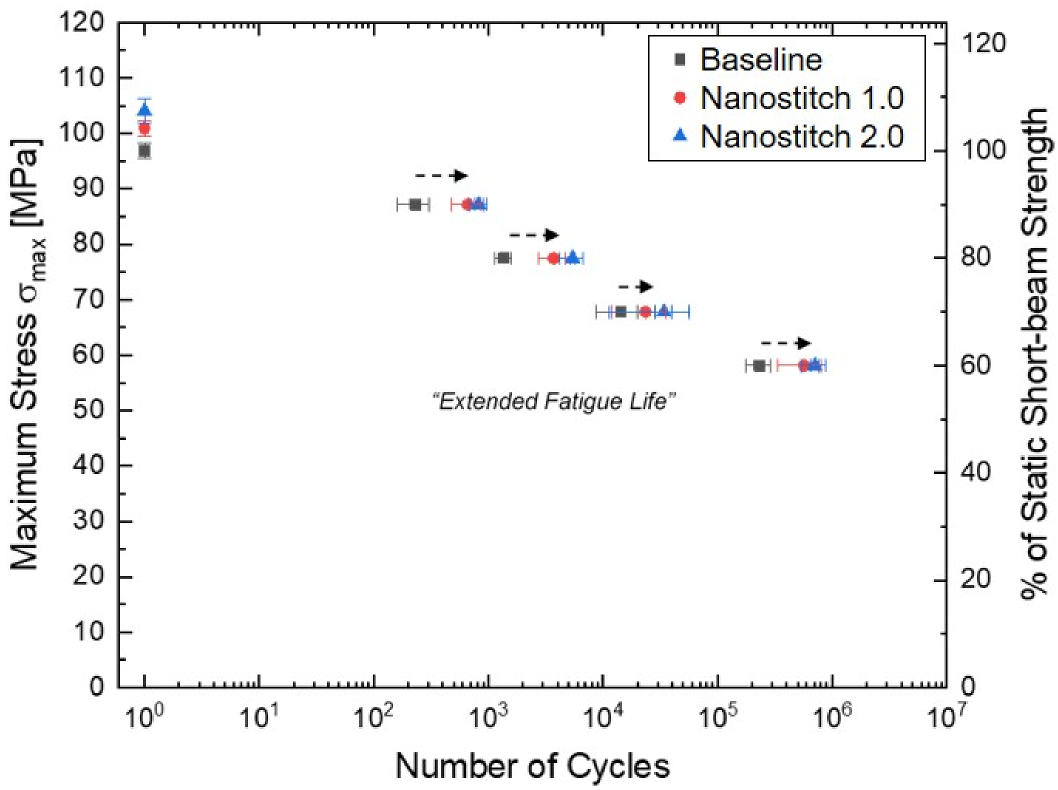

Fig. 5 Fatigue short beam shear test results of baseline, nanostitch 1.0, and nanostitch 2.0. The nanostitch 1.0 and nanostitch 2.0 exhibit extended fatigue life compared to baseline.

Of note, while nanostitch 2.0 outperform nanostitch 1.0 in mean values, there was no statistical difference between them. Details for the fatigue life of each stress level are provided in Table 1. The measured fatigue life of IM7/8552 baseline specimens are consistent with the previously reported values [21]. The fatigue specimens failed catastrophically, corresponding to a sudden damage event in a brittle manner with no prior indication such as audible indications and reaching maximum displacement limit. Such failure modes observed in this work are similar to the results from Ni et al. [22, 23], where a 16-ply quasi-isotropic AS4/8552 laminate was used. Figure 6 shows the representative 2D μCT slices of post mortem SBS specimens. The μCT scan revealed that the damage mode was changed due to the interlaminar reinforcements. While the baseline specimen showed clear and straight damage at the middle of the specimen where the maximum shear stress occurs, the nanostitch 1.0 and nanostitch 2.0 specimens showed a diffusive damage mode. The diffusive cracks infer that the crack propagation with nanostitches is accompanied by an increase in total crack length and the number of plies involved in crack propagation. This more diffusive behavior suggests that the reinforced interlaminar region is too strong and tough to let cracks propagate through the region; thus, the crack tends to deviate

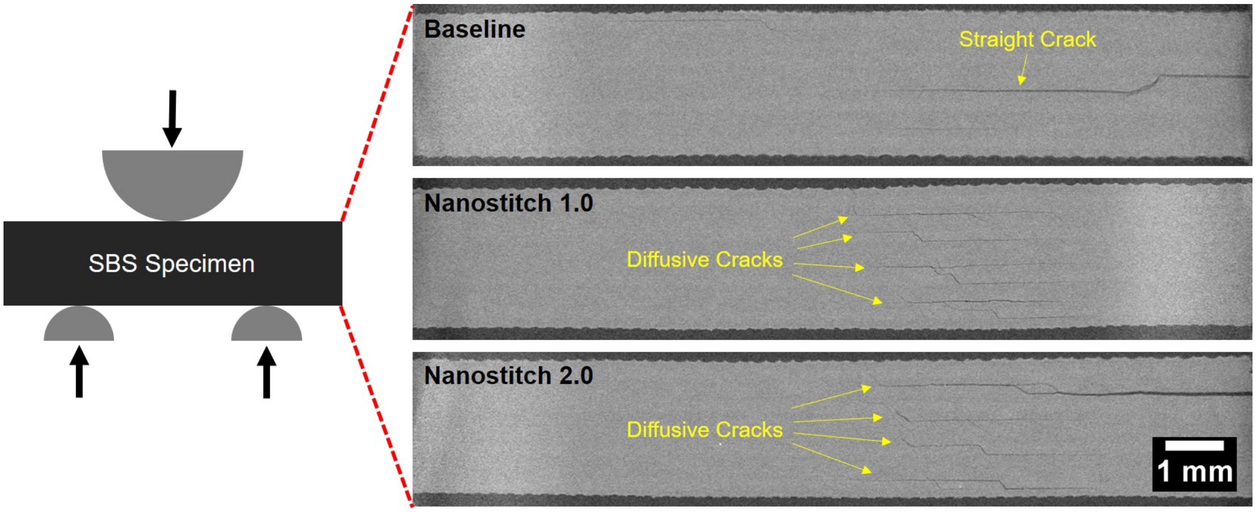

Fig. 6 µCT images of *post mortem* short beam shear specimens. While the baseline showed a straight crack mode, the nanostitch 1.0 and 2.0 specimens showed diffusive crack modes.

through the relatively weaker regions (i.e., the intralaminar region). Also, this observation corroborates the previous study on nanostitch that the interlaminar crack bifurcates into the intralaminar region from the interlaminar precrack, and then propagates within the intralaminar region parallel to the nanostitched interlaminar region [24]. The increased static and fatigue performance of nanostitch 2.0 can be attributed to the twice higher CNT density in the interlaminar region than nanostitch 1.0. Future work should explore the individual effects of buckling and patterning of VACNT (nanostitch 2.0) via parametric approaches. For example, nanosittch 2.0 with an even higher volume fraction would support the effect of CNT density on the mechanical properties.

V. Conclusion

In summary, a multi-level hierarchy is demonstrated in advanced composite laminates with vertically aligned carbon nanotube (VACNT) arrays in order to fabricate next-generation composite architectures. The hierarchical nano- and micro-engineered interlaminar reinforcement comprised of VACNTs were introduced in advanced aerospace-grade composite laminates (i.e., HexPly IM7/8552) by integrating (1) buckling of VACNT arrays to make use of energy dissipation of the wavy nanofibers (e.g., during pulling out), and (2) patterning of VACNT arrays to facilitate higher volume fraction of CNTs. The integration of buckled and patterned VACNTs shows ~7% increase in static interlaminar shear strength and a ~224% increase in fatigue life under short beam shear tests, compared to the baseline. These hierarchical interlaminar reinforcements modified the damage modes from monotonic and straight cracks to a more diffusive *post mortem* set of cracks, resulting in a significant increase in structural strength. This work demonstrates the ability to utilize structural instability of the nanoscale fibers at the microscale, and suggests new insights and opportunities on how to toughen composite laminates.

Acknowledgments

This material is based upon work supported by the Naval Air Warfare Center under Contract No. N68335-19-C-0409. This work was also supported in part by the U. S. Army Research Laboratory and the U. S. Army Research Office through the Institute for Soldier Nanotechnologies under contract number W911NF-13-D-0001. Micro-computed tomography instrumentation support by the Office of Naval Research (ONR) under grant number ONR.N000141712068 through the Defense University Research Instrumentation Program (DURIP) is gratefully acknowledged. The authors gratefully acknowledge the members of necstlab for technical support and advice. This work was carried out in part through the use of MIT's Microsystems Technology Laboratories.

References

[1] Irving, P. E., and Soutis, C., *Polymer composites in the aerospace industry*, Woodhead Publishing, 2019.

[2] Tong, L., Mouritz, A. P., and Bannister, M., *3D fibre reinforced polymer composites*, Elsevier, 2002.

[3] Dransfield, K. A., Jain, L. K., and Mai, Y.-W., "On the effects of stitching in CFRPs—I. Mode I delamination toughness," *Composites Science and Technology*, Vol. 58, No. 6, 1998, pp. 815–827.

[4] Jain, L. K., Dransfield, K. A., and Mai, Y.-W., "On the effects of stitching in CFRPs—II. Mode II delamination toughness," *Composites Science and Technology*, Vol. 58, No. 6, 1998, pp. 829–837.

[5] Mouritz, A., Leong, K., and Herszberg, I., "A review of the effect of stitching on the in-plane mechanical properties of fibre-reinforced polymer composites," *Composites Part A: applied science and manufacturing*, Vol. 28, No. 12, 1997, pp. 979–991.

[6] Larsson, F., "Damage tolerance of a stitched carbon/epoxy laminate," *Composites Part A: applied science and manufacturing*, Vol. 28, No. 11, 1997, pp. 923–934.

[7] Partridge, I. K., and Cartié, D. D., "Delamination resistant laminates by Z-Fiber® pinning: Part I manufacture and fracture performance," *Composites Part A: applied science and manufacturing*, Vol. 36, No. 1, 2005, pp. 55–64.

[8] Fiedler, B., Gojny, F. H., Wichmann, M. H., Nolte, M. C., and Schulte, K., "Fundamental aspects of nano-reinforced composites," *Composites science and technology*, Vol. 66, No. 16, 2006, pp. 3115–3125.

[9] Gorbatikh, L., Wardle, B. L., and Lomov, S. V., "Hierarchical lightweight composite materials for structural applications," *Mrs Bulletin*, Vol. 41, No. 9, 2016, pp. 672–677.

[10] Garcia, E. J., Wardle, B. L., and Hart, A. J., "Joining prepreg composite interfaces with aligned carbon nanotubes," *Composites Part A: Applied Science and Manufacturing*, Vol. 39, No. 6, 2008, pp. 1065–1070.

[11] Gibson, R. F., "A review of recent research on mechanics of multifunctional composite materials and structures," *Composite structures*, Vol. 92, No. 12, 2010, pp. 2793–2810.

[12] Li, H., Xu, Z.-H., and Li, X., "Multiscale hierarchical assembly strategy and mechanical prowess in conch shells (Busycon carica)," *Journal of structural biology*, Vol. 184, No. 3, 2013, pp. 409–416.

[13] Zbib, A., Mesarovic, S. D., Lilleodden, E., McClain, D., Jiao, J., and Bahr, D., "The coordinated buckling of carbon nanotube turfs under uniform compression," *Nanotechnology*, Vol. 19, No. 17, 2008, p. 175704.

[14] Cao, A., Dickrell, P. L., Sawyer, W. G., Ghasemi-Nejhad, M. N., and Ajayan, P. M., "Super-compressible foamlike carbon nanotube films," *Science*, Vol. 310, No. 5752, 2005, pp. 1307–1310.

[15] Hutchens, S. B., Hall, L. J., and Greer, J. R., "In situ mechanical testing reveals periodic buckle nucleation and propagation in carbon nanotube bundles," *Advanced Functional Materials*, Vol. 20, No. 14, 2010, pp. 2338–2346.

[16] Chen, X., Beyerlein, I. J., and Brinson, L. C., "Curved-fiber pull-out model for nanocomposites. Part 1: Bonded stage formulation," *Mechanics of materials*, Vol. 41, No. 3, 2009, pp. 279–292.

[17] Chen, X., Beyerlein, I. J., and Brinson, L. C., "Curved-fiber pull-out model for nanocomposites. Part 2: Interfacial debonding and sliding," *Mechanics of Materials*, Vol. 41, No. 3, 2009, pp. 293–307.

[18] Lee, J., Stein, I. Y., Devoe, M. E., Lewis, D. J., Lachman, N., Buschhorn, S. T., Kessler, S. S., and Wardle, B. L., "Impact of carbon nanotube length on electron transport in aligned carbon nanotube networks The MIT Faculty has made this article openly available . Please share Citation and Brian L . Wardle . " Impact of Carbon Nanotube Length on Publisher Version Access," *Applied Physics Letters*, Vol. 106, No. 5, 2015, pp. –. https://doi.org/http://dx.doi.org/10.1063/1.4907608, URL http://scitation.aip.org/content/aip/journal/apl/106/5/10.1063/1.4907608.

[19] Johnson, W., and Mangalgiri, P., "Investigation of fiber bridging in double cantilever beam specimens," *Journal of Composites, Technology and Research*, Vol. 9, No. 1, 1987, pp. 10–13.

[20] ASTM-D2344, "Standard test method for short-beam strength of polymer matrix composite materials and their laminates. ASTM International, West Conshohocken PA, 2006," , 2006.

[21] Lewis, D. J., "Interlaminar reinforcement of carbon fiber composites from unidirectional prepreg utilizing aligned carbon nanotubes," Master's thesis, Massachusetts Institute of Technology, 2016.

[22] Ni, X., Furtado, C., Kalfon-Cohen, E., Zhou, Y., Valdes, G. A., Hank, T. J., Camanho, P. P., and Wardle, B. L., "Static and fatigue interlaminar shear reinforcement in aligned carbon nanotube-reinforced hierarchical advanced composites," *Composites Part A: Applied Science and Manufacturing*, Vol. 120, 2019, pp. 106–115.

[23] Ni, X., Acauan, L. H., and Wardle, B. L., "Coherent nanofiber array buckling-enabled synthesis of hierarchical layered composites with enhanced strength," *Extreme Mechanics Letters*, Vol. 39, 2020, p. 100773. https://doi.org/https://doi.org/10.1016/j.eml.2020.100773, URL http://www.sciencedirect.com/science/article/pii/S235243162030105X.

[24] Ni, X., Furtado, C., Fritz, N. K., Kopp, R., Camanho, P. P., and Wardle, B. L., "Interlaminar to intralaminar mode I and II crack bifurcation due to aligned carbon nanotube reinforcement of aerospace-grade advanced composites," *Composites Science and Technology*, Vol. 190, 2020, p. 108014. https://doi.org/https://doi.org/10.1016/j.compscitech.2020.108014, URL http://www.sciencedirect.com/science/article/pii/S0266353819336383.